Effect of Strain on the Epitaxy of B-Doped $Si_{0.5}Ge_{0.5}$ Source/Drain Layers

G. Rengo[a,b,c], C. Porret[b], A. Y. Hikavyy[b], E. Rosseel[b], M. Ayyad[b], R. J. H. Morris[b], G. Pourtois[b,d], R. Loo[b], and A. Vantomme[a]

[a] Quantum Solid-State Physics, KU Leuven, Celestijnenlaan 200D, 3001 Leuven, Belgium
[b] Imec, Kapeldreef 75, 3001 Leuven, Belgium
[c] FWO - Vlaanderen, Egmontstraat 5, 2000 Brussel, Belgium
[d]Plasmant, University of Antwerp, 2610 Wilrijk-Antwerpen, Belgium

The impact of strain on the growth of *in situ* boron doped $Si_{0.5}Ge_{0.5}$ epitaxial layers is discussed. The lattice strain has been varied by changing the $Si_{0.5}Ge_{0.5}$ thickness and by growing the epitaxial layer on strain relaxed substrates with different Ge concentrations. With decreasing compressive strain, the B incorporation reduces, and the Ge concentration increases. Through density functional theory calculations, the dependence on the applied strain of the energetic cost for boron incorporation into the $Si_{0.5}Ge_{0.5}$ surface was investigated.

Introduction

The progressive downscaling of field-effect transistor (FET) devices is nowadays hindered by the raise in parasitic resistances which makes performance improvements difficult to achieve. In particular, the contact resistance (R_c) at the source/drain (S/D) contacts has become the major component among the parasitics, due to the continuous contact area (A_c) shrinkage (1). To keep this resistance sufficiently low, materials must be engineered to reduce the specific contact resistivity (ρ_c) of the metal/semiconductor stack. In ohmic contacts, ρ_c is linked to the Schottky barrier height ($q\phi_B$) and to the semiconductor carrier concentration (N) via the expression: $\rho_c \propto \exp(q\phi_B/\sqrt{N})$ (2). The need for ultra-low ρ_c therefore initiated renewed efforts to achieve the highest possible active doping concentration in the region of the semiconductor adjacent to the contact.

In pMOS devices, boron doped $Si_{1-x}Ge_x$ is typically used as a S/D material. Due to its larger lattice parameter than silicon, it induces a compressive strain in the channel region that enhances the holes mobility, leading to an overall improvement in the device performances (3). It also enables higher metastable $[B]_{act}$ values than those obtained for pure Si and Ge. The highest B levels reported in literature are close to 10^{21} at./cm^3 and were obtained for Ge concentrations between 50% and 70% (4). However, despite these interesting features, a further increase of the electrically active doping concentration is needed to realize contacts with ρ_c below 1 x 10^{-9} Ω.cm^2, a value indicated as the milestone for enabling devices beyond the 5 nm node (5).

Several groups have shown that, in nanoscale 3D structures, the misfit biaxial strain in $Si_{1-x}Ge_x$/Si heterostructures is hardly maintained due to the elastic relaxation at the free surfaces (6,7). In addition to a detrimental effect on the channel properties, it also affects

the solid solubility of dopants in semiconductors (8). For instance, the compressive strain in $Si_{1-x}Ge_x$ is alleviated by the presence of boron atoms in substitutional position and this elastic energy reduction is reflected in an enhancement of the B solubility (9). Therefore, it is important to understand how the expected strain variations will affect the epitaxial growth processes in future device architectures. Reactions occurring at the growing surface during the chemical vapor deposition (CVD) of Si:B / Si(001) in presence of B_2H_6 have been described in literature (10). However, to the best of the authors' knowledge, a description of the interaction of this precursor with the $Si_{1-x}Ge_x$ surface is still missing.

This paper describes the impact of strain on the growth of *in situ* boron doped $Si_{0.5}Ge_{0.5}$. The study is two-fold: experimental results are first used to describe how the epitaxial growth and the chemical composition of $Si_{0.5}Ge_{0.5}$:B layers vary with the strain state of the growing layer. In the second part, *ab initio* density functional theory (DFT) calculation results are discussed to illustrate how the B_2H_6 decomposition on a $Si_{0.5}Ge_{0.5}$ surface and the B incorporation in the layer are affected by the strain level and strain type (compressive versus tensile).

Experimental details

Epitaxy and characterization methodology

B doped $Si_{0.5}Ge_{0.5}$ epitaxial layers were grown in an ASM Intrepid® production cluster on blanket n-type Si(001) substrates or commercially available $Si_{1-y}Ge_y$(001) strain-relaxed buffers (SRBs) with different Ge contents (25%, 50%, and 70%) (11). The cluster includes two epi reactors and an integrated pre-epi clean module (Previum®). The Si wafer received a high temperature bake (1050°C) in a reduced pressure of H_2 to remove the native oxide. Since this temperature is not compatible with $Si_{1-x}Ge_x$ materials, the SRB substrates underwent a low temperature plasma treatment in the Previum® chamber prior to deposition (12).

All depositions were done by co-flowing conventional precursors such as dichlorosilane ($Si_2Cl_2H_2$), germane (GeH_4), HCl, and diborane (B_2H_6) for the *in situ* B doping. The growth was performed at 550°C and a pressure of 20 Torr.

Surface morphologies were inspected by top-view scanning electron microscopy (SEM) using a KLA-Tencor eDR7100™ electron-beam wafer defect review system. Reciprocal space maps (RSM) were acquired around the asymmetric Si(113) Bragg reflection with a Bruker JVX7300M diffractometer, using a Cu $K_{\alpha 1}$ source (λ = 1.5406 Å) and a two-bounce Ge(220) monochromator. From the RSM, the degree of strain relaxation and the Ge concentration of the epilayers was extracted using a simulation software from Bruker based on the Bragg's law and the modified Vegard's law (13) combined with the Poisson ratio to determine the out of plane lattice constant of the materials. The boron chemical concentrations ($[B]_{chem}$) in the epilayers were measured by secondary ion mass spectroscopy (SIMS) using a CAMECA® SC-Ultra system with an O_2^+ primary beam at an impact energy of 350 eV. In order to quantify the B atomic concentration, five boron implants of known fluence in $Si_{1-x}Ge_x$ with different but known stoichiometry were measured, thus allowing the $[B]_{chem}$ quantification through polynomial fitting. Thicknesses of the layers were also extracted through the crater depth measurement. The Ge

concentrations in the samples were measured by Rutherford backscattering spectroscopy (RBS) in random geometry. The incident beam of He^+ ions was produced with a 5SHD-2 linear Pelletron Accelerator manufactured by NEC. An incident energy of 1.57 MeV was used, and the backscattered ions were collected at a glancing-exit angle.

Density functional theory calculations

Ab initio DFT calculations were performed using the Gaussian and Plane-Wave method (GPW) (14) implemented in the Quickstep module of the CP2K software package (15). Simulations were run using the generalized gradient approximation with a modified Perdew-Burke-Ernzerhof exchange correlation functional (PBEsol) (16)(17). The DZVP-MOLOPT-GTH (valence double zeta plus polarization, molecularly optimized) basis sets (18), ideal for calculating properties in gas and condensed phase, were used to describe the electronic density of the atoms present in the system and combined with the pseudopotentials derived by Goedecker-Teter-Hutter (GTH) (19). The cut-offs used for the real space integration of the electronic densities and the Gaussian functions are 350 and 30 Ry, respectively. To sample the Brillouin zone, a 2×2×1 Monkhorst-Pack integration grid is used (20). The electronic temperature has been set to 300 K. For the boron adsorption and incorporation simulations, a $Si_{0.5}Ge_{0.5}$(001) slab model with eight monoatomic layers and 16 atoms per layer has been developed, in which the Germanium atoms have been distributed randomly. The surface is 2x1 reconstructed and passivated by a hydrogen monolayer. Periodic boundary conditions have been applied to the supercell. In the z-direction the slab is separated from its nearest replica by a 29 Å thick vacuum region. Molecules included in the calculations, namely B_2H_6, BH_3, and H_2, underwent geometry optimization in simulation boxes large enough to avoid interaction with their nearest images. Van der Waals correction schemes (Grimme D3 (21)) were tested on some configurations to verify the impact on calculated enthalpies of formation. Since the energy values were not significantly affected by the corrections, they have not been applied to the calculations here reported.

Results and discussion

Impact of starting template on $Si_{0.5}Ge_{0.5}$ growth

In reference (22), we describe how the incorporation of B and Ge during the $Si_{1-x}Ge_x$ epitaxy on Si substrates is affected by strain relaxation of the growing layer. As an example, Fig. 1a shows the SIMS spectrum as measured for a partially relaxed boron doped $Si_{0.5}Ge_{0.5}$ layer grown on a Si substrate. In the lower part of the layer (33 – 55 nm) both the Ge concentration (x_{Ge}) and $[B]_{chem}$ are constant, except for a B-overshoot at the interface with the substrate, which is caused by an (avoidable) instability in gas pressure when the growth is started. However, in the top 33 nm of the layer, x_{Ge} and $[B]_{chem}$ are not constant. x_{Ge} gradually increases and $[B]_{chem}$ decreases towards the surface. By changing the epi-layer thickness, it has been demonstrated that the variation in Ge and B incorporation coincides with the initiation of strain relaxation during $Si_{1-x}Ge_x$ growth (18). In the first ~2 nm, the quantification of both B and Ge is hindered by the near-surface transient distortion (23). This part is consequently disregarded in the following discussions.

The variation in $[B]_{chem}$ as a function of layer thickness, i.e., the degree of strain relaxation is also reflected in the electrical properties of $Si_{1-x}Ge_x$:B thin films and in the contact properties of $Si_{1-x}Ge_x$:B/Ti stacks (18). Figure 1b shows the resistivity (ρ) and the contact resistivity (ρ_c) as a function of layer thickness, in other words for layers with a different degree of strain-relaxation. The lowest ρ and ρ_c values are obtained for a fully strained 23 nm thick $Si_{0.5}Ge_{0.5}$ layer. Once the metastable critical thickness is exceeded (~25 nm in case of $Si_{0.5}Ge_{0.5}$), both ρ and ρ_c increase with thickness. For the thinnest layer, surface scattering effects play an important role, causing an increase in both ρ and ρ_c. For $Si_{1-x}Ge_x$ layers with a lower Ge concentration (not shown here), the critical thickness is higher and ρ and ρ_c show a plateau as long as the layer thickness does not exceed the metastable critical thickness for strain relaxation (18).

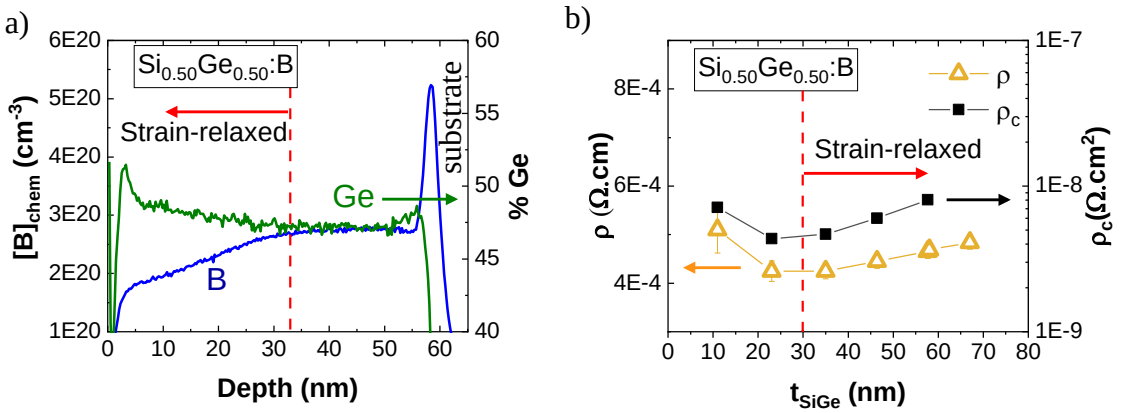

Figure 1. a) B and Ge concentration profiles as measured by SIMS in a partially relaxed $Si_{0.5}Ge_{0.5}$:B epi-layer (18). The region of the layer between the interface with the substrate and the vertical dashed line was grown while being fully strained. The part of the layer on the left side of the red dashed line was deposited after the initiation of strain relaxation. b) ρ and ρ_c as measured for $Si_{0.5}Ge_{0.5}$:B / Ti contacts as a function of the $Si_{0.5}Ge_{0.5}$:B layer thickness (18). The red dashed line indicates the thickness at which strain-relaxation starts to occur.

A similar effect of strain relaxation on material composition has been reported for GeSn, with a spontaneous-relaxation-enhanced Sn incorporation (24–26). An explanation, based on thermodynamic considerations, has been proposed, which links this behaviour to the hindrance of Sn incorporation by the compressive strain present in the material. However, besides the effects of the strain induced by lattice mismatch, local strain fields created by misfit and threading dislocations need to be considered. These local strain variations alter the surface morphology, eventually affecting the material composition during the growth. In this work, this latter effect has been ruled out. The magnitude and sign of the strain have not been varied by inducing strain relaxation in the layers, but by growing $Si_{0.5}Ge_{0.5}$:B epilayers on $Si_{1-y}Ge_y$ SRBs with different compositions (y = 0, 0.25, 0.5, or 0.70). Figure 2 reports the names of the samples, the corresponding stack description, and the strain statuses of the epilayers. By tuning the lattice mismatch between the SRB and the epilayer, it is possible to induce compressive, no-, or tensile strain in the epilayer. The very low threading dislocation density (TDD) in the stack (11) allows to attribute differences in the properties of the grown materials exclusively to the different strain present. The $Si_{0.5}Ge_{0.5}$:B epilayers have a nominal thickness of 60 nm and a $[B]_{chem}$ of 3 x 10^{20} cm^{-3}.

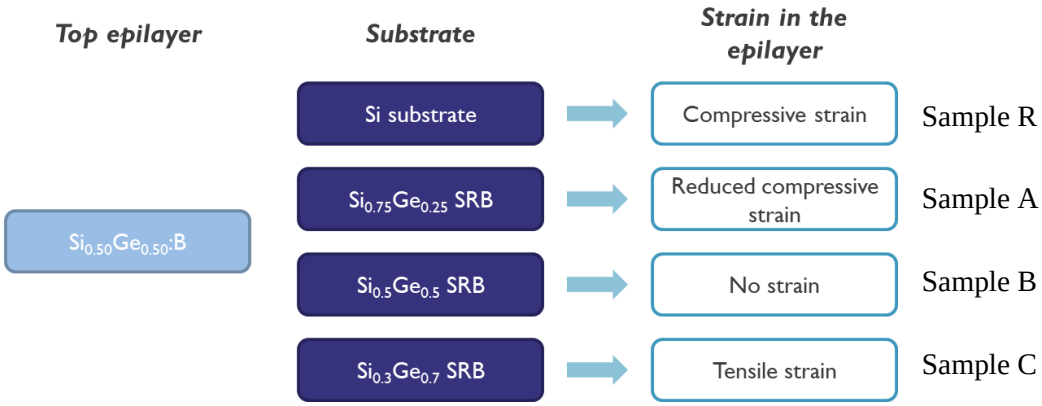

Figure 2. Strain status in the grown epilayers as defined by the mismatch with the underlying virtual substrate.

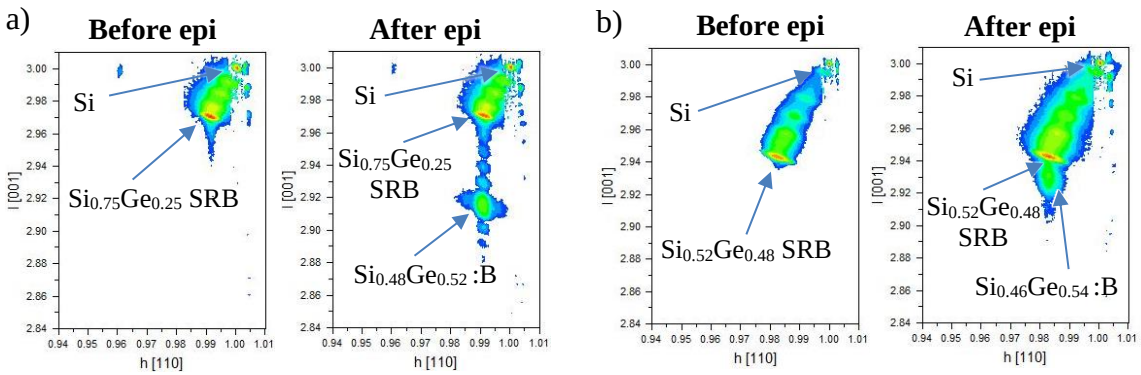

Figure 3. Reciprocal space maps acquired around the Si(113) Bragg reflection for nominal $Si_{0.5}Ge_{0.5}$:B epilayers grown on $Si_{1-y}Ge_y$ SRBs with a) y = 0.25 and b) y = 0.5, acquired before and after epitaxial deposition.

Figure 3 shows the RSMs around the (113) Bragg reflection of Si as obtained for $Si_{0.5}Ge_{0.5}$:B layers grown on SRBs with y = 0.25, and y = 0.50, respectively. Labels indicate the diffraction peaks of the Si substrate, the $Si_{1-y}Ge_y$ SRB, and the $Si_{1-x}Ge_x$ epilayer. The step-graded Ge profile of the SRB signature is clearly recognized (11). The peak with the highest intensity corresponds to the top layer of the SRB. The SRBs are nearly fully relaxed. In Figure 3a - after epi, as expected, the epilayer peak is located below the $Si_{0.75}Ge_{0.25}$ diffraction peak, confirming its larger out of plane lattice constant. In Figure 3b, the epilayer peak was ideally supposed to overlap with that of the SRB as the nominal x_{Ge} was 0.50 for both. Instead, their position differ slightly. A Ge fraction of ~ 0.48 has been extracted for the SRB top layer, and ~ 0.54 for the epilayer. It is also noticed that the extracted x_{Ge} in the grown layer progressively increases with increasing y_{Ge} in the SRB. For the examples shown in Figure 3, the peaks assigned to the $Si_{0.5}Ge_{0.5}$:B epilayers appear at the same *h* coordinates as the top of the underlying SRBs, meaning that their in-plane lattice parameters match. These epilayers are therefore fully strained with respect to the underlying SRB. The layer grown on Si has, instead, a degree of relaxation of 25%. However, before reaching the critical thickness, the layer had grown pseudomorphically, while containing the highest compressive strain among all the samples here reported. The region of the layer adjacent to the substrate is therefore relevant for comparison with the layers grown on SRBs. The extracted Ge concentrations and degrees of relaxation for the

virtual substrates and for the epilayers are reported in TABLE I. The relaxation is indicated with respect to Si for the SRB top layers, and with respect to the SRB for the epilayers.

TABLE I. Ge concentrations and degrees of strain relaxation of the virtual substrates and the epilayers as extracted from RSMs.

	SRB			**Epilayer**		
Sample	**Nominal material**	**y_{Ge}**	**Degree of Relaxation (%)**	**Nominal material**	**x_{Ge}**	**Degree of Relaxation [*wrt* SRB]**
R	Si	0	100	$Si_{0.5}Ge_{0.5}$:B	0.48	25%
A	$Si_{0.75}Ge_{0.25}$	0.25	94	$Si_{0.5}Ge_{0.5}$:B	0.52	~0%
B	$Si_{0.5}Ge_{0.5}$	0.48	97	$Si_{0.5}Ge_{0.5}$:B	0.54	~0%
C	$Si_{0.3}Ge_{0.7}$	0.66	99	$Si_{0.5}Ge_{0.5}$:B	NA	NA

Figure 4a compares the B concentration depth profiles as extracted by SIMS for the B-doped $Si_{1-x}Ge_x$ epitaxial layers grown on Si and on the different SRBs. The B incorporation during epitaxial growth is clearly affected by the magnitude and the type of the biaxial strain. The highest B concentrations have been measured for the compressively strained $Si_{0.5}Ge_{0.5}$ layers. It is, however, remarkable that the $Si_{0.5}Ge_{0.5}$ layer grown on the SRB with 25% Ge contains a similar boron level to the layer grown on the Si substrate. This is also the case just above the substrate/epitaxial interface, i.e. when the $Si_{0.5}Ge_{0.5}$ layer grown on Si was still fully strained. As expected from 25 nm above the interface on, the boron incorporation decreases due to the onset of strain relaxation. In the nominally unstrained layer, the $[B]_{chem}$ is significantly lower. The $Si_{0.5}Ge_{0.5}$ grown on the $Si_{0.3}Ge_{0.7}$ SRB has the lowest $[B]_{chem}$ of ~ 2 x 10^{19} cm^{-3}. This indicates that the tensile strain is detrimental for B incorporation.

The Ge concentration in the epilayer, as extracted from RBS, is also significantly affected by the starting template. It, however, shows an opposite trend compared to $[B]_{chem}$, with a monotonic increase in x_{Ge} as the compressive strain is reduced and tensile strain introduced. Results from this assessment are summarized in TABLE II. The $Si_{1-x}Ge_x$ layer grown on the $Si_{0.5}Ge_{0.5}$ SRB for instance presents a Ge fraction being 8% higher than that of the epilayer grown on Si.

Finally, the growth rates of the epilayers are also significantly impacted. Since B doping is known to enhance the growth rate in the CVD of Si (27), the reduction in boron incorporation with reducing the compressive strain may explain the significant decrease in growth rate from sample A to B. As different starting substrates could affect the surface temperature during growth, resulting in the differences evidenced above, surface temperatures were monitored used a pyrometer during the process. Temperature differences were found to be very limited, in the order of 1-2°C, which rules out a significant impact on the epitaxial growth process.

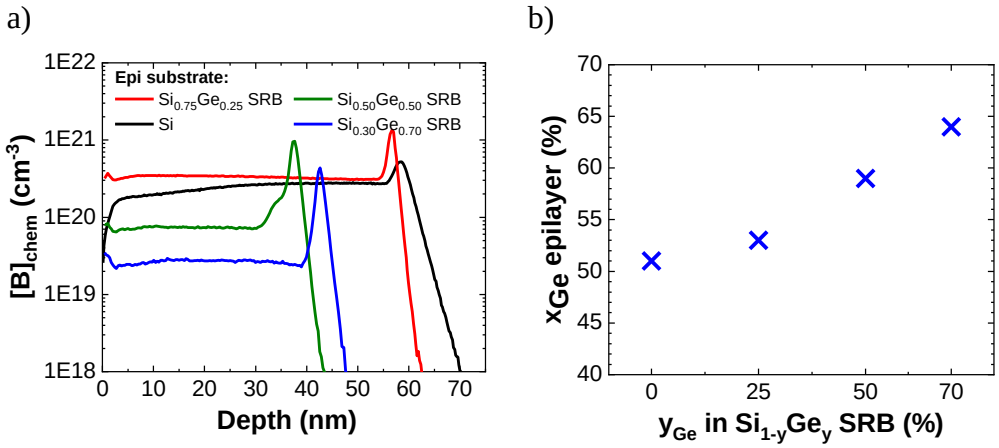

Figure 4.a) SIMS boron concentration profiles as measured for the epilayers of the samples. b) Epilayers Ge concentrations as measured with RBS.

TABLE II. Layer thicknesses and $[B]_{chem}$ as extracted from SIMS, and Ge concentrations measured by RBS.

Sample	Thickness (nm)	Growth rate (nm/min)	$[B]_{chem}$ (cm^{-3})	x_{Ge}
R	59	6.8	2.7×10^{20}	0.51
A	56	6.7	3.0×10^{20}	0.53
B	37	4.4	7.3×10^{19}	0.59
C	43	5.2	2.7×10^{19}	0.64

DFT modelling of B_2H_6 decomposition and B incorporation at the $Si_{0.5}Ge_{0.5}$ surface

Atomistic DFT calculations were used to investigate the adsorption and decomposition of diborane on a (001) oriented $Si_{0.5}Ge_{0.5}$ surface and to predict how these processes are affected by different strain levels. A schematic of the typical slab model is shown in Figure 5a. The models are built starting from an eight atomic layers thick Si(001) slab. The exposed surfaces are 2x1 reconstructed and contain 16 Si atoms per layer, framed in two rows of four dimers each. Both the bottom and top surfaces are fully H-passivated. The interaction between the top surface and the B_2H_6 molecule is studied, while the bottom surface remains untouched. After atomic positions and cell optimizations, in-plane supercell dimensions of 15.41 Å and 15.16 Å are obtained for x and y, respectively. The Si atoms in the slab are then randomly replaced with Ge atoms, with a probability of 50%. A $Si_{0.5}Ge_{0.5}$(001) slab is obtained, with the Si or Ge atoms placed on the sites corresponding to the pure Si lattice. Next, the geometry is optimized again using four different constraint conditions: (i) the atomic positions and lattice parameters are optimized simultaneously to obtain a $Si_{0.5}Ge_{0.5}$ slab without any strain. The relaxed cell expands to 15.80 Å and 15.54 Å in the x and y directions, respectively. (ii) The lattice constants are fixed to match those of the Si slab. The geometry is optimized (atomic positions but not the simulation cell dimensions) and the atomic coordinates of the system expand in the z-direction into the vacuum region. A slab replicating pseudomorphic $Si_{0.5}Ge_{0.5}$(001) is obtained. This system corresponds to the fully-compressively-strained case. For systems (iii) and (iv), two fixed sets of x and y cell dimensions have been chosen, with intermediate values between those of the fully relaxed (i) and the pseudomorphic (ii) cases, after which the atomic positions have been optimized. The obtained strain statuses correspond to 33% and 66% relaxed $Si_{0.5}Ge_{0.5}$ on Si. The stress tensors for the four systems are calculated. The typical tensor

structure corresponds to that of a biaxially strained system, with comparable σ_{xx} and σ_{yy} components and neglectable stress values in all the other components. Details of the four slab models used are summarized in TABLE III.

TABLE III. Strain conditions applied to the slab model

Strain condition	(x,y) cell dimensions (Å^2)	σ_{xx} (GPa)	σ_{yy} (GPa)
Fully-compressively-strained	15.41 x 15.16	4.72	4.03
33% relaxed	15.54 x 15.29	3.06	2.58
66% relaxed	15.68 x 15.43	1.36	1.09
Unstrained	15.80 x 15.54	0.00	0.00

The decomposition pathway of a B_2H_6 molecule on the $Si_{1-x}Ge_x(001)$ surface is considered to proceed in three steps, namely (i) the chemisorption of the B_2H_6 molecule on the surface, (ii) surface reaction, and incorporation in the lattice by either replacing a Ge (iii-a) atom or a Si (iii-b) atom (Figure 5b-e). The surface chemical reactions corresponding to the different steps are indicated in the following. The symbol (s) indicates that the compound is a solid. It is in the gaseous phase otherwise.

$$Si_{0.5}Ge_{0.5}(s) + B_2H_6 \rightarrow Si_{0.5}Ge_{0.5} - B_2H_5(s) + \frac{1}{2}H_2 \quad \text{(i)}$$

$$Si_{0.5}Ge_{0.5}(s) + B_2H_6 \rightarrow Si_{0.5}Ge_{0.5} - BH_2(s) + BH_3 + \frac{1}{2}H_2 \quad \text{(ii)}$$

$$Si_{0.5}Ge_{0.5}(s) + B_2H_6 \rightarrow Si_{0.5}Ge_{0.5(-1Ge\ at.)}{:}B - GeH_2(s) + BH_3 + \frac{1}{2}H_2 \quad \text{(iii-a)}$$

$$Si_{0.5}Ge_{0.5}(s) + B_2H_6 \rightarrow Si_{0.5(-1Si\ at.)}Ge_{0.5}{:}B - SiH_2(s) + BH_3 + \frac{1}{2}H_2 \quad \text{(iii-b)}$$

The formation enthalpy (ΔH_f) for each step with respect to the initial system is given by:

$$\Delta H_{f,step} = (E_{ads} + E_{bypr}) - \left(E_{slab} + E_{B_2H_6}\right) \quad [1]$$

where E_{ads} is the DFT-calculated energy for the SiGe slab with the B_xH_y, GeH_2, or SiH_2 chemisorbed group, E_{bypr} is the energy of the gaseous by-product(s), E_{slab} is the energy of the pristine $Si_{0.5}Ge_{0.5}(001)$ surface slab, and E_{B2H6} is the energy of the gaseous B_2H_6 molecule. This analysis does not consider thermal effects, such as the entropy variation, but provides indications of the most stable equilibrium configurations in the systems slab + adsorbates. However, the epitaxial growth is an out-of-equilibrium process, which cannot be fully described in this way. Nevertheless, the results obtained from DFT modelling still provide information about the driving forces for the layer deposition.

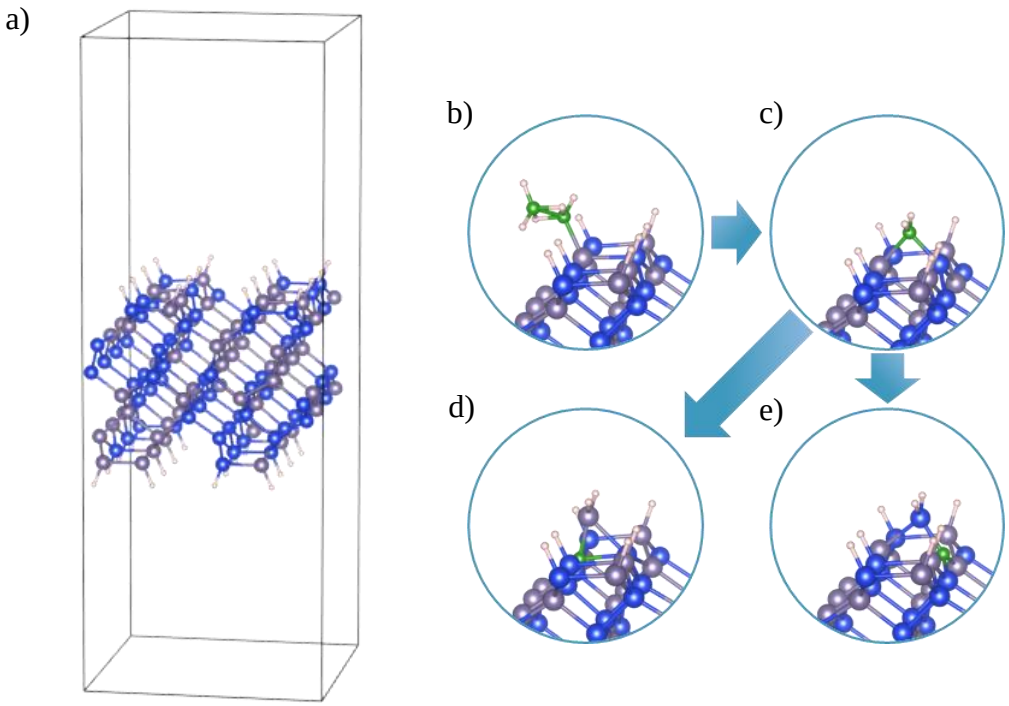

Figure 5.a) $Si_{0.5}Ge_{0.5}$(001)-2x1 surface slab model used in DFT calculations. b) "Adsorption" step. c) "Reaction" step. d) "Incorporation (Ge)" step. e) Incorporation (Si)" step.

Figure 6 shows the formation enthalpies (ΔH_f) calculated for the different steps of the B_2H_6 reaction pathway the $Si_{0.5}Ge_{0.5}$ surface and for applying different magnitudes of strain to the slab. Because the chosen initial system is very stable with a fully hydrogen passivated reconstructed surface, ΔH_f has positive values for all the configurations. In reality, the deposition process proceeds at elevated temperatures and the hydrogen passivation is partially lost thus creating potential adsorption sites for the B_2H_6 molecules. For the adsorption and reaction steps (represented in Figure 5b-c) the calculated ΔH_f is hardly affected by the amount of applied strain. The incorporation of a B atom into the surface is simulated by starting from the "Reaction" configuration and swapping the atomic positions of B and either a Ge atom in the surface dimer (Figure 5d), or a Si atom (Figure 5e) as proposed in (28) for the dissociation of phosphine on a Si(001) surface. Two different configurations are obtained, where the boron atom replaces one of the lattice atoms in a surface dimer and the removed Ge or Si atom is placed on top of the surface as an adatom. In both cases the calculated formation enthalpies vary with the magnitude of compressive strain present in the surface slab. From this result, one can expect that the epitaxy *in situ* boron doped epitaxial $Si_{1-x}Ge_x$ growth is affected by the stain state of the growing layer. A higher incorporation probability of the B atoms is expected during the growth of compressively strained layers with respect to unstrained layers.

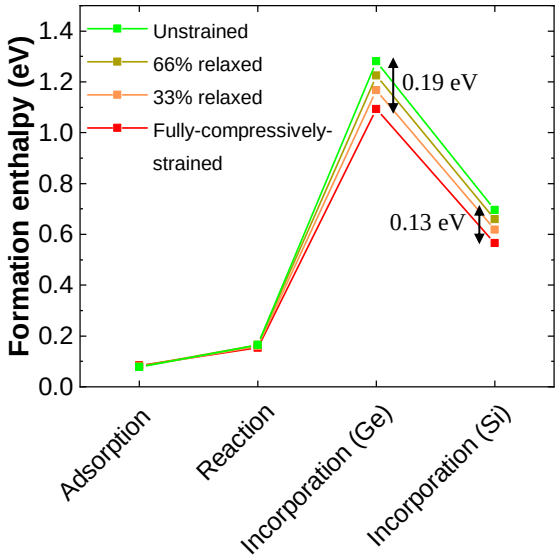

Figure 6. Formation enthalpies calculated for intermediate steps of the B_2H_6 decomposition and B incorporation in $Si_{0.5}Ge_{0.5}$(001) with different strain conditions.

In Figure 7a, we report the evolution of the x-component of the stress in the slab at the various steps of the B_2H_6 decomposition pathway and for different strain states. Positive values correspond to compressive stress, negative to tensile. As expected, the chemisorbed B_xH_y groups have a limited impact on the lattice strain, while the B incorporated into the surface row of the atomic lattice causes a release of the compressive strain. The strain release is larger when a Ge atom is replaced by B, rather than a Si atom. The reduction in stress is highest for the fully compressively strained lattice and decreases with decreasing strain in the starting slab (Fig. 7b). This supports the experimentally observed tendency of B to be incorporated when a compressive strain is present in the growing layer and the increase in x_{Ge} when the compressive strain is not present.

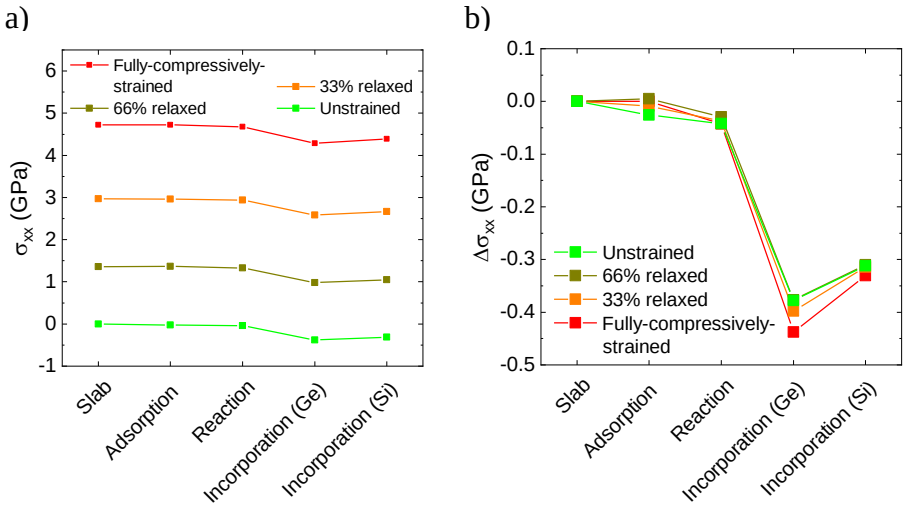

Figure 7. a) x-component of calculated stress in the slabs for the different steps of the considered B_2H_6 decomposition pathway and for different strain conditions. b) Relative variation in the x-component of the stress with respect to that of the pristine surface slab for the different decomposition steps. The four applied strain conditions are reported.

Summary

We have described how strain affects the epitaxial growth process of *in situ* B doped $Si_{0.5}Ge_{0.5}$. In case of compressively strained $Si_{0.5}Ge_{0.5}$:B growth on Si, B and Ge incorporation during the epitaxial growth are affected by the initiation of layer relaxation, i.e., the B (Ge) incorporation decreases (increases) with increasing degree of strain relaxation. The effect of elastic strain on B and Ge incorporation was also observed when modifying the magnitude and sign of the strain by growing B doped $Si_{0.5}Ge_{0.5}$ layers onto $Si_{1-y}Ge_y$ strain relaxed buffers (SRBs) with different compositions.

Through *ab initio* density functional theory calculations, the mechanisms of B_2H_6 decomposition and the effect of strain on the B incorporation into a $Si_{0.5}Ge_{0.5}$(001) surface have been simulated while applying four different strain conditions. The energetic cost to incorporate the B atom into the first atomic layer of the surface varies with the strain applied to lattice. The obtained trends in energetic cost vs strain are in line with the experimental observations. The calculation of the stress evolution in the slab model at the different B_2H_6 reaction steps confirms that B incorporation in the lattice reduces the compressive strain caused by the presence of Ge in the lattice. The change in lattice strain by B incorporation increases with increasing compressive strain implemented in the starting model. The other steps of the reaction pathway do not have a significant impact on the strain in the slab. Therefore, the variation in compressive strain is expected to influence the incorporation probability of boron during the epitaxial deposition, while the surface coverage of B_xH_y-groups is expected to be unaffected by the strain status of the layer.

Acknowledgments

G. Rengo acknowledges the Research Foundation of Flanders (FWO) for granting him a PhD fellowship strategic basic research. The imec core CMOS program members, European Commission, local authorities and the imec pilot line are acknowledged for their support. This project has received funding from the ECSEL Joint Undertaking (JU) under grant agreement No 875999. The JU receives support from the European Union's Horizon 2020 research and innovation programme and Netherlands, Belgium, Germany, France, Austria, Hungary, United Kingdom, Romania, Israel. The imec MSP group is acknowledged for useful weekly discussions. We gratefully acknowledge Qiang Zhao from the QSP unit of KU Leuven for his support with the RBS measurements. The $Si_{1-x}Ge_x$ SRB wafers were provided by Siltronic AG.

References

[1] A. V.-Y. Thean, D. Yakimets, T. Huynh Bao, P. Schuddinck, S. Sakhare, M. G. Bardon, A. Sibaja-Hernandez, I. Ciofi, G. Eneman, A. Veloso, J. Ryckaert, P. Raghavan, A. Mercha, A. Mocuta, Z. Tokei, D. Verkest, P. Wambacq, K. De Meyer, and N. Collaert, *2015 IEEE Symp. VLSI Technol.*, pp. T26–T27 (2015).

[2] S. M. Sze and K. K. Ng, *Physics of Semiconductor Devices*. Hoboken, NJ, USA, 2006.

[3] P. Verheyen, N. Collaert, R. Rooyackers, R. Loo, D. Shamiryan, A. De Keersgieter, G. Eneman, F. Leys, A. Dixit, M. Goodwin, Y. S. Yim, M. Caymax, K. De Meyer, P. Absil, M. Jurczak, and S. Biesemans, *2005 IEEE Symp. VLSI Technol.*, pp. 194–

195 (2005).
[4] R. Loo, A. Y. Hikavyy, L. Witters, A. Schulze, H. Arimura, D. Cott, J. Mitard, C. Porret, H. Mertens, P. Ryan, J. Wall, K. Matney, M. Wormington, P. Favia, O. Richard, H. Bender, A. Thean, N. Horiguchi, D. Mocuta, and N. Collaert, *ECS J. Solid State Sci. Technol.*, **6**(1), pp. P14–P20 (2017).
[5] C.-N. Ni, K. V. Rao, F. Khaja, S. Sharma, S. Tang, J. J. Chen, K. E. Hollar, N. Breil, X. Li, M. Jin, C. Lazik, J. Lee, H. Maynard, N. Variam, A. J. Mayur, S. Kim, H. Chung, M. Chudzik, R. Hung, N. Yoshida, and N. Kim, *2016 IEEE Symp. VLSI Technol.*, pp. 1–2 (2016).
[6] O. Moutanabbir, M. Reiche, W. Erfurth, F. Naumann, M. Petzold, and U. Gösele, *Appl. Phys. Lett.*, **94**(24), pp. 1–4 (2009).
[7] M. Tomita, D. Kosemura, K. Usuda, and A. Ogura, *ECS Trans.*, **53**(1), pp. 207–214 (2013).
[8] C. Ahn, N. Bennett, S. T. Dunham, and N. E. B. Cowern, *Phys. Rev. B - Condens. Matter Mater. Phys.*, **79**(7), pp. 1–4 (2009).
[9] B. Tillack, P. Zaumseil, G. Morgenstern, D. Krüger, and G. Ritter, *Appl. Phys. Lett.*, **67**, pp. 1143–1144 (1995).
[10] Q. Campbell, J. A. Ivie, E. Bussmann, S. W. Schmucker, A. D. Baczewski, and S. Misra, **125**(1), pp. 481–488 (2021).
[11] G. Kozlowski, O. Fursenko, P. Zaumseil, T. Schroeder, M. Vorderwestner, and P. Storck, *ECS Trans.*, **50**(9), pp. 613–621 (2013).
[12] F. Wang, B. B. Jotheeswaran, J. Tolle, X. Lin, P. Gao, and A. Demos, *Solid State Phenom.*, **282**, pp. 25–30 (2018).
[13] J. P. Dismukes, L. Ekstrom, and R. J. Paff, *J. Phys. Chem.*, **68**(10), pp. 3021–3027 (1964).
[14] G. Lippert, J. Hutter, and M. Parrinello, *Mol. Phys.*, **92**(3), pp. 477–487 (1997).
[15] J. Vandevondele, M. Krack, F. Mohamed, M. Parrinello, T. Chassaing, and J. Hutter, *Comput. Phys. Commun.*, **167**(2), pp. 103–128 (2005).
[16] J. P. Perdew, K. Burke, and M. Ernzerhof, *Phys. Rev. Lett.*, **77**(18), pp. 3865–3868 (1996).
[17] J. P. Perdew, A. Ruzsinszky, G. I. Csonka, O. A. Vydrov, G. E. Scuseria, L. A. Constantin, X. Zhou, and K. Burke, *Phys. Rev. Lett.*, **100**(13), pp. 1–4 (2008).
[18] J. VandeVondele and J. Hutter, *J. Chem. Phys.*, **127**(11), p. 114105 (2007).
[19] S. Goedecker and M. Teter, *Phys. Rev. B - Condens. Matter Mater. Phys.*, **54**(3), pp. 1703–1710 (1996).
[20] H. J. Monkhorst and J. D. Pack, *Phys. Rev. B*, **13**(12), pp. 5188–5192 (1976).
[21] S. Grimme, J. Antony, S. Ehrlich, and H. Krieg, *J. Chem. Phys.*, **132**(15), p. 154104 (2010).
[22] G. Rengo, C. Porret, A. Y. Hikavyy, E. Rosseel, N. Nakazaki, G. Pourtois, A. Vantomme, and R. Loo, *ECS Trans.*, **98**(5), pp. 27–36 (2020).
[23] W. Vandervorst, T. Janssens, B. Brijs, T. Conard, C. Huyghebaert, J. Frühauf, A. Bergmaier, G. Dollinger, T. Buyuklimanli, J. A. VandenBerg, and K. Kimura, *Appl. Surf. Sci.*, **231**–**232**, pp. 618–631 (2004).
[24] J. Margetis, S. Al-Kabi, W. Du, W. Dou, Y. Zhou, T. Pham, P. Grant, S. Ghetmiri, A. Mosleh, B. Li, J. Liu, G. Sun, R. Soref, J. Tolle, M. Mortazavi, and S. Q. Yu, *ACS Photonics*, **5**(3), pp. 827–833 (2018).
[25] W. Dou, M. Benamara, A. Mosleh, J. Margetis, P. Grant, Y. Zhou, S. Al-Kabi, W. Du, J. Tolle, B. Li, M. Mortazavi, and S. Q. Yu, *Sci. Rep.*, **8**(1), pp. 1–11 (2018).
[26] S. Assali, J. Nicolas, and O. Moutanabbir, *J. Appl. Phys.*, **125**(2), (2019).

[27] D. Grützmacher, *J. Cryst. Growth*, **182**(1–2), pp. 53–59 (1997).
[28] H. F. Wilson, O. Warschkow, N. A. Marks, S. R. Schofield, N. J. Curson, P. V. Smith, M. W. Radny, D. R. McKenzie, and M. Y. Simmons, *Phys. Rev. Lett.*, **93**(22), pp. 2–5 (2004).